Electrochimica Acta 467 (2023) 143090

Contents lists available at ScienceDirect

Electrochimica Acta

journal homepage: www.journals.elsevier.com/electrochimica-acta

Hydrocarbon-based membranes cost-effectively manage species transport and increase performance in thermally regenerative batteries

Nicholas R. Cross [a], Holkan Vazquez-Sanchez [b], Matthew J. Rau [c], Serguei N. Lvov [d,e,f], Michael A. Hickner [g], Christopher A. Gorski [h], Shashank S. Nagaraja [b], S. Mani Sarathy [b], Bruce E. Logan [a,h], Derek M. Hall [d,e,*]

[a] Department of Chemical Engineering, Pennsylvania State University, University Park, PA 16802, USA
[b] Clean Combustion Research Center, King Abdullah University of Science and Technology, Thuwal 23955, Saudi Arabia
[c] Department of Mechanical & Aerospace Engineering, George Washington University, Washington, DC 20052, USA
[d] The EMS Energy Institute, Pennsylvania State University, University Park, PA 16802, USA
[e] Department of Energy and Mineral Engineering, Pennsylvania State University, University Park, PA 16802, USA
[f] Department of Materials Science and Engineering, Pennsylvania State University, University Park, PA 16802, USA
[g] Department of Chemical & Materials Science Engineering, Michigan State University, East Lansing, MI 48824, USA
[h] Department of Civil and Environmental Engineering, Pennsylvania State University, University Park, PA 16802, USA

ARTICLE INFO

Keywords:
Waste heat
Flow battery
Membrane
Energy efficiency

ABSTRACT

Low-temperature heat (T<130°C) can be utilized by thermally regenerative batteries (TRBs) for power production, allowing the thermal energy to be converted to storable chemical potential energy. However, TRBs suffer from high ohmic losses and ammonia crossover, which has slowed their development. In this study, we examined how the use of six different membranes influenced TRB performance, determined the most influential membrane parameters, and identified promising membrane candidates that cost-effectively increase TRB performance. Of the six membranes examined, an inexpensive, hydrocarbon CEM (Selemion CMVN) had low ammonia crossover without compromising resistance, resulting in good performance across all metrics studied. A thin anion exchange membrane (Sustainion, 50 microns) showed a high peak power density of 82 mW cm^{-2} due to low resistance, but the average power density and energy density were low due to high ammonia flux. Full discharge curves using Selemion CMVN provided an average power density of 26 ± 7 mW cm^{-2} with an energy density of 2.9 Wh L^{-1}, which were large improvements on previous TRBs. A techno-economic analysis showed that Selemion CMVN had the lowest levelized cost of storage ($410 per MWh) at an applied current density of 50 mA cm^{-2}.

1. Introduction

Many different stationary systems such as industrial facilities and thermal powerplants produce large amounts of low temperature heat (T<130°C) that goes unused by waste heat recovery processes [1]. Multiple recent reviews discuss the state of the art for electrochemical waste heat power generation systems [2–6], so here we only discuss the development of the technology specific to this work, thermally regenerative batteries (TRBs). TRBs can take advantage of this low-temperature heat to produce power and store energy for the grid [2–7]. A TRB is a type of redox flow battery that is recharged with low-temperature waste heat rather than electric energy through electrolyte chemistry modifications. A thermally separable ligand, such as ammonia, ethylenediamine, or acetonitrile, is added to one electrolyte to change the electrochemical equilibrium potential of a redox reaction of interest. The presence of the ligand in one electrolyte creates the potential difference between the two electrodes, allowing power and energy to be discharged from the battery. Once the battery is discharged, the ligand can be thermally separated from the electrolyte to recharge the battery using low-temperature heat (Fig. 1a), meaning that the low-grade heat harvesting and power production systems are completely decoupled and that the flow battery operates under isothermal conditions (for a detailed schematic, see our previous work [8]). The ability to store ligands for later use enables TRBs to also function as energy storage

* Corresponding author at: The EMS Energy Institute, Pennsylvania State University, University Park, PA 16802, USA.
E-mail address: dmh5373@psu.edu (D.M. Hall).

https://doi.org/10.1016/j.electacta.2023.143090
Received 15 June 2023; Received in revised form 25 August 2023; Accepted 26 August 2023
Available online 27 August 2023

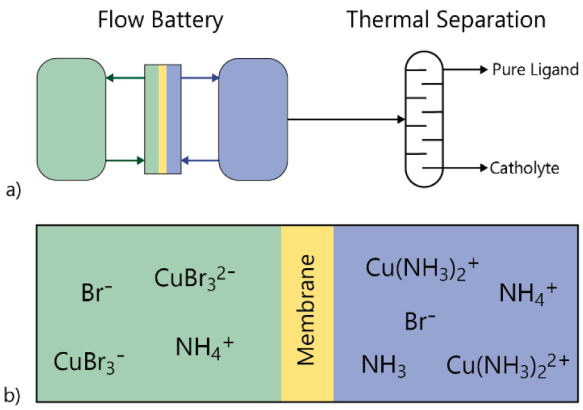

Fig. 1. Schematic of (a) the Cu_{aq}-TRAB system process and (b) the species present in Cu_{aq}-TRAB electrolytes.

devices. Ammonia has been the most promising ligand so far due to its relatively lower thermal energy required for regeneration, high metal-ligand solubility, and low conductivity losses [9–12]. Single-metal ammonia TRBs have used copper and silver as the redox active metal that undergoes deposition-dissolution reactions [13], but are limited by unstable electrode materials [14–16], low power and energy density, and deposition uniformity [17–20]. Bimetallic ammonia TRBs use zinc and copper to increase the cell potential difference, but have more complex system design and still have thermodynamic instability issues [21–25]. The all-aqueous copper thermally regenerative ammonia battery (Cu_{aq}-TRAB) has been shown to have high power and energy output with stable oxidation states, resulting in favorable power densities and energy efficiencies with a simple system design [8,26].

The Cu_{aq}-TRAB performs poorly in key metrics needed to achieve levelized costs of storage (LCOS) competitive with conventional flow batteries and other waste heat power systems. A recent study has shown that for all ranges of discharge times, maximizing power density was the main driver for decreasing LCOS [27]. The major power and energy bottleneck for the Cu_{aq}-TRAB has been the membrane as it has caused two major issues: diffusive ammonia transport causing energy losses [8], and low conductivity causing power losses [28]. Recent approaches on metal-based copper TRABs to reduce the impact of ammonia crossover has had some success through methods such as an extra chamber for holding the ammonia and an additional membrane with a sacrificial electrolyte, but both have resulted in larger ohmic losses and lower power output [29–33]. Another approach based on removal of the membrane for development of microfluidic flow channels reduces ohmic losses, but energy density is lower due to fast crossover and power density is still low due to the use of planar rather than porous electrodes [34,35]. Some custom-made membranes have increased battery power and energy, but these membranes cannot be purchased at commercial scales and have not shown high long-term stabilities [15,36].

Previous flow battery studies examining different membranes have shown that there is a large impact of electrolyte composition and charge carrier on membrane performance [37]. For Nafion membranes, the presence of ammonia and ammonium salts significantly decrease the membrane conductivity [38,39]. Possible reasons for this are the relationship between dominant charge carrier size and ionic conductivity in the membrane and osmotic swelling due to high ionic strength of the electrolyte [40,41]. Past studies that have compared cation and anion exchange membranes in vanadium redox flow batteries have shown that simply changing the membrane charge while keeping the backbone the same did not improve vanadium crossover because of the decreased impact of Donnan exclusion in high ionic strength electrolytes [42,43]. However, specific anion exchange membranes can reduce vanadium crossover while having low resistance [44], implying that ion transport control is membrane material and electrolyte chemistry specific. Uncharged, thin-film composite membranes have demonstrated high performance in vanadium redox flow batteries with high power and energy density due to size exclusion permitting passage of primarily protons with low vanadium leakage [45,46]. Like most TRBs, the Cu_{aq}-TRAB electrolytes have high ionic strengths (>5 M) and two different pH values (catholyte ~4, anolyte ~9). Given, the range of aqueous species present, it is not clear which membrane type would be most appropriate for this battery (Fig. 1b). In the Cu_{aq}-TRAB, the ammonia molecule is uncharged and is unlikely to be impacted by the charge of the membrane, but transport could be inhibited by size-exclusion membranes.

A better understanding is needed of the factors influencing membranes used in Cu_{aq}-TRABs. We evaluated several different types of membranes for their impacts on battery performance and energy storage cost through symmetry cell and full cell experiments. We examined three membrane types: cation, anion, and uncharged membranes, with two membranes from each category to quantify their power and energy density in the Cu_{aq}-TRAB. Next, we investigated the underlying transport mechanisms that govern the relationship between membrane characteristics and battery performance. Lastly, we analyzed the levelized cost of energy storage for each membrane studied for short and long discharges to demonstrate the tradeoffs between battery performance and membrane cost. These results can be extended to other flow battery chemistries that use non-traditional electrolytes and help inform future membrane choice and design.

2. Materials and methods

Salts used for all tests were ammonium bromide (99%, Thermo Scientific), sodium chloride (99%, Sigma Aldrich), copper (I) bromide (98%, Alfa Aesar), copper (II) bromide (99%, Acros Organics), zinc bromide (98%, Thermo Fisher Scientific), and sucrose (99%, Thermo Scientific). The source of ammonia was a 28 wt% ammonium hydroxide solution (Thermo Scientific). All electrolytes were purged with argon (99.997%, Praxair) to prevent undesired oxidation of the copper during testing. The electrodes were carbon felt (AvCarb G280A) and were thermally treated at 400°C for 5 hours before testing. Membranes were chosen to represent each major membrane type (cation, anion, and size-exclusive) and were stored as recommended by the manufacturer upon receipt and tested without modification (Table 1).

All full cell battery tests were run using a 25 cm^2 column-pin flow field (FuelCellStore) on a graphite plate in a flow-through configuration. The electrolytes were prepared such that the initial state of charge was 100%: the catholyte contained all Cu(II), and the anolyte contained all Cu(I), with an argon purge of each electrolyte to prevent oxygen

Table 1
Membranes studied and pertinent information regarding each type.

Membrane	Dry Thickness (μm)	Cost ($ cm^{-2})	Composition	Membrane Type
Nafion 117	175	0.05	Teflon backbone with sulfonic acid groups	CEM
Selemion CMVN	85	0.027	Hydrocarbon backbone with Na^+ counter ion	CEM
Sustainion E30-50 Grade T	50	0.69	Teflon support with triethylamine charge groups	AEM
Selemion AMVN	100	0.027	Polyolefin backbone with Cl^- counter ion	AEM
FilmTec BW30	150	0.013	Polyamide thin film transport layer with polysulfone and PET support layers	Uncharged
FilmTec NF270	140	0.013	Polyamide thin film transport layer with polysulfone and PET support layers	Uncharged

contamination. The catholyte and anolyte (50 mL each) were pumped into the reactor stack at 50 mL min^{-1} using a peristaltic pump. Even pressure and compression was applied to the flow cell using a torque wrench set to 2.5 Nm. The gaskets used were 2 mm thick, which compressed the carbon felt electrodes by approximately 30%. Electrochemical characterizations were completed using a Gamry Reference 3000. Polarization curves were obtained by linearly sweeping the cell potential from the open circuit potential to 0 V at a sweep rate of 25 mV s^{-1}. The power density was calculated by the product of the current and the voltage, normalized to the projected cell area. Discharge curves were conducted at 10 mA cm^{-2} with a cutoff voltage of 0.65 V unless otherwise specified. To provide a performance metric to describe battery power output during discharge for battery scale-up purposes (similar to "rated" or "nominal" power for a large-scale stack), the average power density during the discharge curve was presented with the error being one standard deviation from the average. The energy density, ($\widehat{U}_{exp}$) was calculated by

$$\widehat{U}_{exp} = \frac{\int P\ dt}{V_{tot}} \tag{1}$$

where P is the power output (W) at time t and V_{tot} is the total volume of electrolyte used (anolyte plus catholyte, 100 mL).

For measuring the flux of each species of interest, a similar electrolyte was present on the opposite side of the membrane with only the species of interest swapped for a similar species to match ionic strength and osmotic pressure (for detailed schematics, see Fig. S1). For catholyte copper flux tests, both electrolytes contained 5 M NH_4Br, the source electrolyte contained 0.5 M $CuBr_2$, and the sink electrolyte instead contained 0.5 M $ZnBr_2$. For anolyte copper flux tests, the same setup was used, but both electrolytes also contained 4 M NH_3. The copper content was measured in the sink electrolyte as a function of time using a UV-Vis spectrophotometer (Shimadzu UV-1800) (calibration data shown in Fig. S6). For ammonium bromide flux tests, the source electrolyte contained 5 M NH_4Br, and the sink electrolyte contained 5 M NaCl. The ammonium and bromide contents were measured in the sink electrolyte as a function of time using ion chromatography (Thermo Scientific ICS-6000). Calibration curves were used to convert the peak area to concentration at each time point when solution was drawn from the sink electrolyte (Fig. S2). Ammonia flux was measured using a pH meter with the pH being converted to ammonia concentration by the Henderson-Hasselbalch equation. Due to the pH of the solution being ~9, the hydroxide concentration was multiple orders of magnitude below the ammonia concentration; therefore, the pH change was caused by ammonia crossover modifying the ammonia/ammonium acid/base equilibrium. This was confirmed by running a test with no ammonia or ammonium species present and creating a pH gradient between the electrolytes using sodium hydroxide and hydrochloric acid. The measured hydroxide flux was less than 5% of what was measured for experiments with ammonia present (Fig. S3). Flux experiments were run using a flow cell (5 cm^2) to prevent damage to the polyamide layer of the uncharged membranes. No electrodes were present during the experiments and no current was applied to ensure that what was being measured was purely membrane diffusion. The solutions were pumped at 15 ml min^{-1} through the flow cell. The flux was calculated simply as the change in species concentration from one time point to the next, normalized to the projected geometric area of the cell.

For a comparison of thermal-to-electric conversion efficiencies from this TRAB to other low-grade heat to electrical energy devices, we used the ratio of the electrical energy density discharged from a TRAB for the configuration specified ($\widehat{U}_{exp}$) and the heat energy input required to complete a thermal separation of ammonia from water (E_{heat})

$$\eta_{heat} = \frac{\widehat{U}_{exp}}{E_{heat}} \tag{2}$$

E_{heat} values have ranged from 100-200 Wh L^{-1} [23,47] depending on the solution composition and column parameters. Our recent work identified 107 Wh L^{-1} as the heat energy input required for 4 M NH_3 under optimized column inlet temperature at atmospheric pressure (see Table S1 of [28]), so this value of E_{heat} was used for this approach.

An alternative method for calculating thermal-to-electric energy conversion was recently proposed in Refs. [2] and [3] and these sources provide a framework to compare devices if some employ multi-effect combination and heat recovery schemes (MEHRS). This modified energy efficiency, η_*, was defined as

$$\eta_* = \eta \frac{\Delta T_{HE} + \Delta T_*}{T_H - T_L} \tag{3}$$

where T_H is the hot side temperature (100°C [28,48–50]), T_L is the cold side temperature (25°C), ΔT_{HE} is the heat exchanger temperature difference (5°C) [2,3], and ΔT_* is the temperature difference needed to complete the thermal separation process (75°C) [2,3]. Using $\Delta T_{HE} = 5$ K, $\Delta T_* = 75$ K, $T_H = 378$ K, and $T_L = 293$ K, modified energy efficiencies were estimated to range from 2.7 – 6.7% for different applied current densities using Selemion CMVN (Table 2). To be consistent with the formulation of this modified energy efficiency with previous work as shown in Fig. 7 of Ref. [2], we used ΔT_* as the difference between the reboiler (373 K) and condenser (298 K) temperatures, T_H was the reboiler temperature + ΔT_{HE}, and the condenser temperature was T_L + ΔT_{HE}.

Membrane resistance in each electrolyte was measured in an "H-cell" (1 cm^2) using electrochemical impedance spectroscopy (EIS). Measurements were taken every 30 minutes for eight hours to allow for the membrane to equilibrate in the electrolyte, then the average steady state resistance value was used as the cell resistance. The cell resistance was converted to membrane specific resistance by removing the membrane and running EIS on the cell without the membrane and converted to membrane area specific resistance,

$$R_{mem} = \left(R_{cell} - R_{cell,\ nomem}\right)A \tag{4}$$

where R_{mem} is the membrane area specific resistance, R_{cell} is the cell resistance with the membrane, $R_{cell,nomem}$ is the cell resistance without the membrane, and A is the area of membrane exposed to the electrolyte [51].

The water uptake of each membrane was estimated for each electrolyte by measuring the mass change of the membrane after equilibration in the electrolyte and the dry membrane weight,

$$\lambda = \frac{m_{wet} - m_{dry}}{m_{dry}} \tag{5}$$

where λ is the water uptake, m_{wet} is the weight of the wet membrane, and m_{dry} is the weight of the dry membrane [51]. The membrane was soaked overnight in the electrolyte of interest for equilibration and any electrolyte on the surface of the membrane was dried with a paper towel to ensure measuring just the weight of the hydrated membrane. The membrane was then washed with DI water to remove any salt and dried overnight before measuring the weight of the dry membrane. Three trials were completed for each membrane and electrolyte.

The techno-economic analysis (TEA) was performed based on the Cu_{aq}-TRAB to determine the levelized cost of storage (LCOS) as the key economic indicator [27]. The LCOS was computed as follows:

Table 2
Energy efficiencies of the Cu_{aq}-TRAB with Selemion CMVN at different applied current densities.

Current Density (mA cm^{-2})	10	30	50	100
η (%)	7.1	6.1	5.5	2.9
η^* (%)	6.7	5.7	5.2	2.7

$$\text{LCOS}\left[\frac{\$}{\text{MWh}}\right] = \frac{\text{CAPEX} + \sum_n^N \frac{\text{O\&M cost}}{(1+r)^n} + \sum_n^N \frac{\text{Charging cost}}{(1+r)^n} + \frac{\text{End}-\text{of}-\text{life cost}}{(1+r)^{N+1}}}{\sum_n^N \frac{\text{Elec}_{\text{Discharged}}}{(1+r)^n}} \quad (6)$$

where r is the discount rate, *N* is the total years of the system lifetime, and *n* is the current year of analysis. Different elements take part, such as the investment cost or capital expenditure (CAPEX), the operation and maintenance (O&M), charging costs, end-of-life cost, and the total electricity discharged throughout its entire lifetime. Further details of the cost breakdown and analysis can be found in the supplementary information (Table S1) and in previous work [27]. A cost inventory was collected from diverse sources and real bulk quotations from the market. Two main scenarios were analyzed: power applications (0.02 h – 0.50 h) and energy applications (1 h – 15 h), where the discharge times varied (for more detailed values, see Table S1). A 20-year project was selected considering some degradation rates for a standard redox flow battery. These include the round-trip efficiency, cycle degradation, time degradation and self-discharge rates.

3. Results and discussion

3.1. Full cell performance

Power curves at full state of charge showed that the Selemion CMVN and Sustainion membranes exhibited the highest peak power densities of 84 and 82 mW cm^{-2} (Fig. 2a). These peak power densities were four times larger than the previous best for a single-metal TRAB [28]. Polarization curves showed that these membranes were able to sustain high cell current densities because of low ohmic resistance (see Section 3.3 and Fig. S4). The Selemion AMVN and BW30 membranes had the lowest peak power densities of 17 mW cm^{-2} (AMVN) and 19 mW cm^{-2} (BW30). Nafion 117 had a peak power density of 27 mW cm^{-2}, and this could be increased by ~25% by using thinner Nafion 115 [26]. However, a thinner membrane will decrease energy density due to increased ammonia crossover (see Section 3.2). In terms of peak power, there was no correlation to which general membrane type (cation, anion, uncharged) performs best because one cation and one anion membrane outperformed their counterparts. Membrane thickness was weakly correlated to the peak power density with thinner membranes generally performing better, but this is likely because previous research has shown that the Cu_{aq}-TRAB is an ohmic-dominated system [28]; therefore, any small improvements to conductivity (e.g. a thinner membrane or one with lower ohmic resistance) will show large gains to peak power density.

There was also no clear trend between peak power density obtained from polarization curves and the energy density obtained during constant-current discharge tests (Fig. 2b). The Sustainion membrane had low energy density, likely because it was the thinnest membrane tested, and thinner membranes increase ammonia crossover (see Section 3.2). The thickness of Nafion 117 (212 microns, Table 1) caused it to have high energy density despite higher ohmic losses because of the longer diffusion length preventing parasitic ammonia crossover. While BW30 had the lowest energy density, it still performed on a similar order of magnitude to other membranes. Overall, membrane thickness showed little correlation with energy density, indicating that chemical differences between membranes were the driving factor for transport control.

The best performing membrane (Selemion CMVN) was tested further to evaluate its performance at high applied current densities (>10 mA cm^{-2}, Fig. 3a). The lowest applied current density (10 mA cm^{-2})

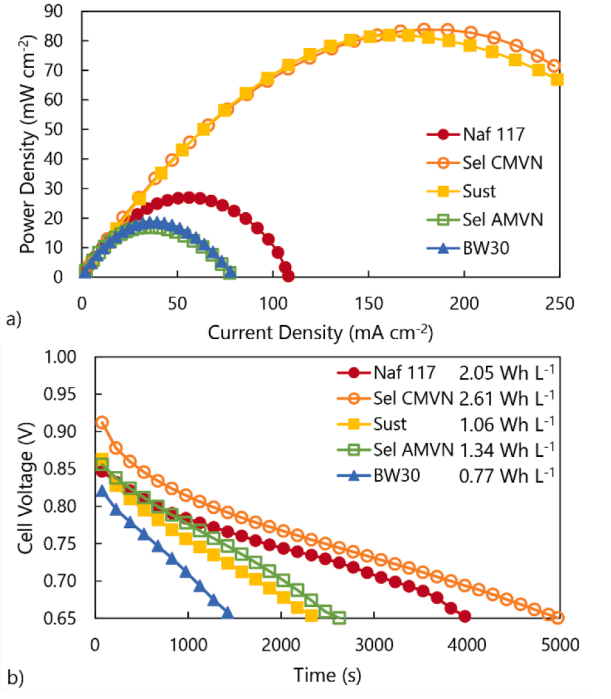

Fig. 2. (a) Power and (b) discharge curves for each membrane tested. Electrolytes were 0.5 M $CuBr_{1/2}$, 5 M NH_4Br, 4 M NH_3 (anolyte only).

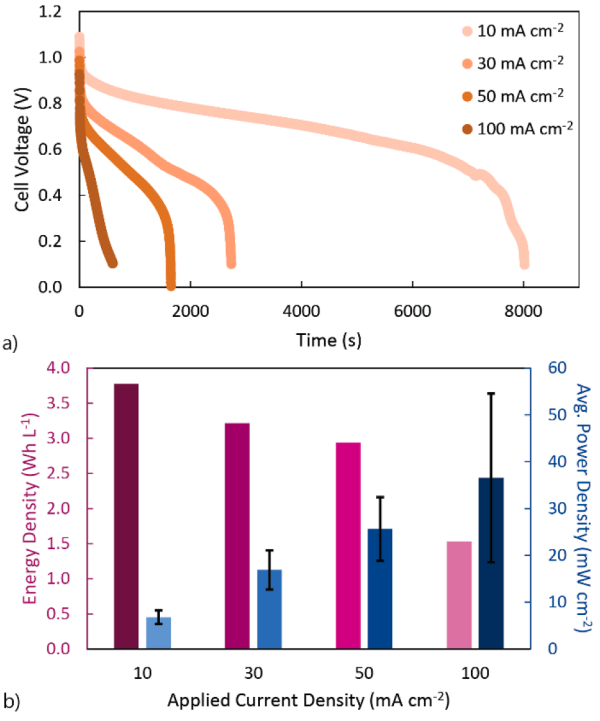

Fig. 3. (a) Discharge curves for Selemion CMVN at varying applied current densities; (b) Comparison of energy density and average power density for Selemion CMVN at varying applied current densities.

resulted in an energy density of 3.8 Wh L^{-1}, which equates to an energy efficiency (η) of 7.1% and modified energy efficiency (η_*) of 6.7% (the highest reported efficiencies for any TRAB are currently $\eta = 2.2\%$ and $\eta_* = 0.9\%$ [2,8]). Discharging at 50 compared to 10 mA cm^{-2} resulted in a 3.75x increase in average power density with only a 22% decrease in energy density. Increasing the current density to 100 mA cm^{-2} increased average power density to 36 mW ± 18 cm^{-2} (Fig. 3b), which is 5.5 times larger than the average power densities previously obtained for these systems [28] but decreased the energy density to 1.5 Wh L^{-1}. Standard deviation of the power density increased significantly at higher applied current densities, but this was likely due to the small volume of electrolyte in the reservoirs leading to short discharge times. Given that the previous *peak* power density of the Cu_{aq}-TRAB was 23 mW cm^{-2} [28], producing greater *average* power output than the previous peak represents a significant advancement in the this technology. Additionally, previous electrochemical waste heat-to-power technologies have been limited to membrane and heat exchanger-normalized power densities below 10 mW cm^{-2} and standard and modified energy efficiencies below 4% (Table 2 and S2) [2]. Therefore, the use of Selemion CMVN as the membrane for the Cu_{aq}-TRAB significantly surpassed these previous limitations.

3.2. Diffusion experiments

Ammonium ions had the highest flux through all membranes tested, indicating that it was the primary ion for passing charge in the Cu_{aq}-TRAB (Fig. 4a), and there was a strong correlation between high ammonium flux and high peak power density. For cation exchange membranes, ammonium flux was 12-21 times greater than bromide flux, while for anion exchange membranes, ammonium flux was only 1.5-3.6 times higher. The decrease in ratio of ammonium to bromide flux demonstrated that membrane charge can still influence ion transport despite the high ionic strength. For the uncharged membranes, the ammonium flux was approximately 4.5 times greater than that of bromide with the primary reason for higher ammonium flux was likely its smaller ionic radius (1.48 Å) than bromide (1.95 Å) [40,52]. Similar flux trends were noticed for copper species diffusion through all membranes with copper flux through Sustainion being high and Selemion AMVN being low, although the flux was multiple orders of magnitude lower due to the large size of the copper-ligand complexes (Fig. S6a and b) [52]. Selemion AMVN showed low fluxes for all species, with there being untraceable copper crossover after multiple days of testing. Thus, while it may have performed poorly in full cell tests and is not best-suited for single-metal TRBs, it could have potential uses where transport control and species separation are more critical for applications where an electrochemical charging is used, such as bimetallic-TRABs.

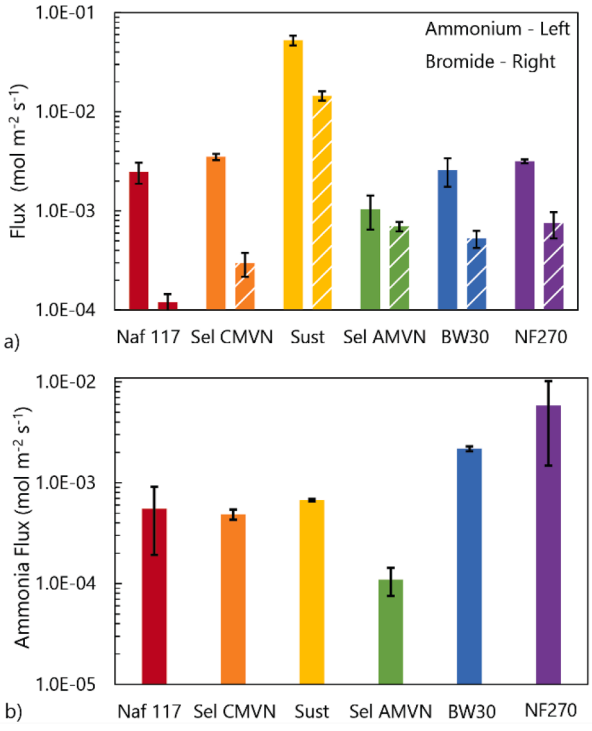

Fig. 4. Flux of (a) ammonium and bromide and (b) ammonia through each membrane.

Membranes with the highest ammonia flux had the lowest energy densities. Ammonia flux was highest through the uncharged membranes (Fig. 4b) and was consistent with BW30 having the shortest discharge time of the membranes studied. Sustainion showed the highest flux of all charged membranes, which was consistent with it having the lowest energy density of the charged membranes. The high ammonia flux also impacted the polarization curve produced by the Sustainion membrane by decreasing the open circuit potential and therefore the peak power density, despite the very high ammonium and bromide fluxes (Fig. S4). Despite Nafion 117 being the thickest membrane tested, it did not have the lowest ammonia flux, indicating that ammonia permeability was high and that while using thinner versions of Nafion would result in higher power output, there would certainly be decreases in energy density. Ammonia flux through Selemion AMVN was half an order of magnitude lower than all other membranes, which is what helped increase the discharge time and energy density, despite the low ionic flux observed for this membrane. Additionally, this indicates that Selemion AMVN would be the best of the membranes studied here for electric charge/discharge cycling of the battery since it would best prevent parasitic diffusive losses over successive cycles. Selemion CMVN had surprisingly low ammonia flux, given its smaller thickness and higher ammonium flux. Comparing Selemion CMVN and AMVN, the 15 μm larger thickness of AMVN would not be enough to warrant the half order of magnitude decrease in ammonia flux. Provided that ammonia is not impacted by the membrane charge, this suggests that the modification of the membrane charge also resulted in smaller pores in the membrane. This observation is supported by Selemion AMVN having the excellent transport control of the larger copper-ligand complexes (Figs. S6a and b) [52]. Further investigation into the relationship between membrane chemical composition and physical structure and the resultant transport properties are of great interest but beyond the scope of this current analysis as a first principles understanding of membrane transport in high ionic strength solutions has yet to be developed.

3.3. Resistance and uptake

Membranes with lower area specific resistances had higher peak power densities, but membrane water uptake was not as well correlated with full cell performance. The area specific resistance of all charged membranes was lower than that of the uncharged membranes (Fig. 5a). Sustainion had the lowest area specific resistance, an average of 0.15 Ω cm^2 in both electrolytes, which was consistent with the high ionic flux and peak power density. However, despite its resistance being ~10% of Selemion CMVN, the peak power of these two membranes was similar, likely resulting from the high ammonia flux through Sustainion, suggesting there was a mixed potential at the positive electrode during full cell testing of Sustainion. While Sustainion had high ammonia flux, the membrane could be incorporated into other previous TRAB cell configurations such as the ammonia breathing structure and sacrificial electrolyte that were limited by high ohmic losses, but the configurations significantly decreased ammonia crossover. The area specific resistance of Nafion was higher than Selemion CMVN, which is likely related to the low ammonium flux observed and is consistent with previous literature that has shown that Nafion conductivity in ammonium-based electrolytes is lower than strong acid electrolytes [38]. Selemion CMVN exhibited a lower resistance in the Cu_{aq}-TRAB

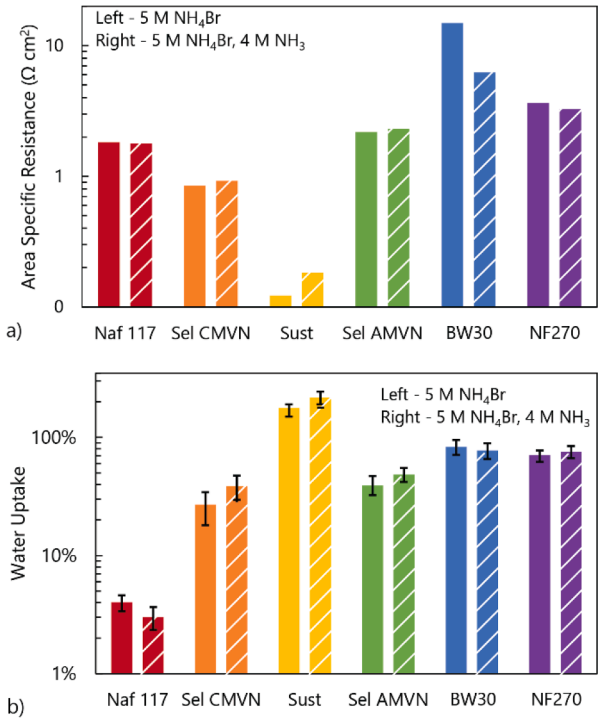

Fig. 5. (a) Area specific resistance and (b) water uptake in 5 M NH_4Br and 5 M NH_4Br + 4 M NH_3

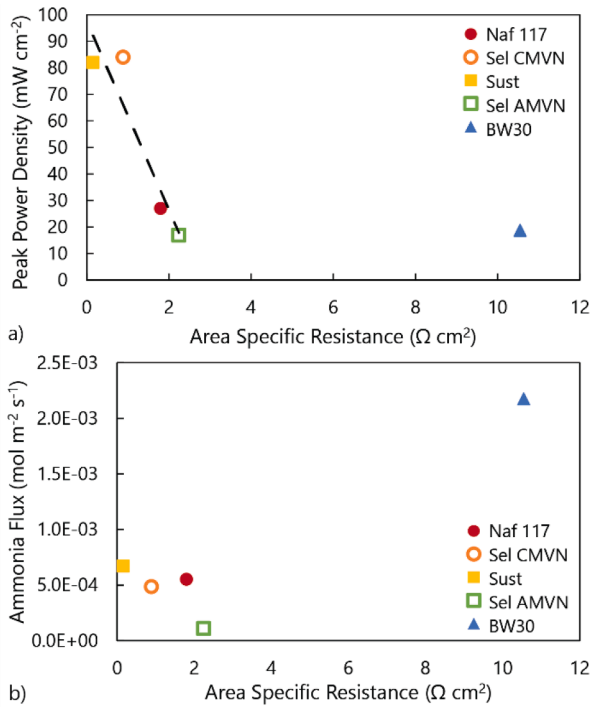

Fig. 6. Comparisons of (a) peak power density and (b) ammonia flux against area specific resistance. Dashed line in figure a) is simply for reference to qualitatively demonstrate linearity of variables correlated (BW30 outlier omitted).

electrolytes than Nafion, which is the opposite of what has been previously demonstrated in strong acid electrolytes (such as sulfuric acid) [53] but is consistent with Selemion membranes showing high conductivity in ammonium-based electrolytes [54]. Most membranes showed little difference in resistance in catholyte or anolyte, with the only exception of the BW30 which had lower resistance in the anolyte.

Sustainion averaged 197% water uptake in both electrolytes, which was by far the highest of all membranes studied (Fig. 5b). High water uptake was related to the high ionic flux through Sustainion since the membrane was well-hydrated and therefore had many channels available for ion transport. Nafion 117 had the lowest water uptake (3.5%), which was consistent with it having high resistance in the Cu_{aq}-TRAB electrolytes, and with previous literature showing that water activity is strongly related to ionic flux and resistance for this membrane [41,55]. Selemion AMVN had a uptake of 44% on average between both electrolytes, which was higher than expected considering its high resistance and low ionic flux. This water uptake was similar to its counterpart, CMVN (33%), again suggesting that Donnan exclusion played a role in decreasing ammonium flux through AMVN, therefore causing it to have a higher resistance. The uncharged membranes showed very high water uptake because a majority of their volume is the porous support layers which swell significantly but play little role in species transport. However, the high water uptake could have helped offset the high resistance of BW30 and be related to the high peak power density observed for this membrane.

3.4. Correlation of symmetry cell to full cell performance

There was a strong correlation between membrane properties and symmetry cell performance to peak power density. For ion exchange membranes, peak power density was found to be related to area specific resistance, with only the BW30 membrane being an outlier (Fig. 6a). The Sustainion peak power density was lower than expected given its low area specific resistance, but this was likely because of the high ammonia flux that caused the mixed potential at the positive electrode. It is unknown why the BW30 peak power density was so high given the low area specific resistance, but it could have been related to the support layer being able to supply embedded ions to the electrolyte to give the appearance of higher conductivity for the short duration that was the polarization curve.

Correlating energy density with membrane properties was not as straightforward as power density because high energy density requires a combination of low resistance and good transport control, which often are in competition of one another by creating mixed potential at the electrodes due to crossover. The BW30 membrane had high resistance and ammonia flux, and thus had the lowest energy density studied (Fig. 6b). Comparing the two anion exchange membranes, Sustainion had very low resistance and high ammonia flux, while Selemion AMVN had the inverse. Thus, they both had lower energy densities than the cation exchange membranes. Given the very low ammonia flux through Selemion AMVN, if the membrane were able to be made at half the thickness (thereby doubling the ammonia flux and halving the resistance), the power density would double and the energy density would potentially increase because of the lower resistance and still low ammonia flux. Selemion CMVN had a good balance of low resistance and low ammonia flux, and therefore had the highest peak power and energy densities of all membranes studied. Overall, the results and testing methods presented here can be used to evaluate and identify future membranes for the Cu_{aq}-TRAB to continue to reduce ohmic losses and increase battery power and energy density.

3.5. Economic analysis

The levelized cost of storage (LCOS) of the Selemion CMVN significantly outperformed other membranes tested in both short- and long-duration discharge scenarios, which is consistent with previous results that show that membrane cost and power density were the primary drivers of LCOS in the Cu_{aq}-TRAB [27]. For power applications, the LCOS for Selemion CMVN was minimized to $438 per MWh at 0.50 hours of discharge time, which was approximately 65% less than the next best membrane, BW30 (Fig. 7a). While Selemion CMVN also had

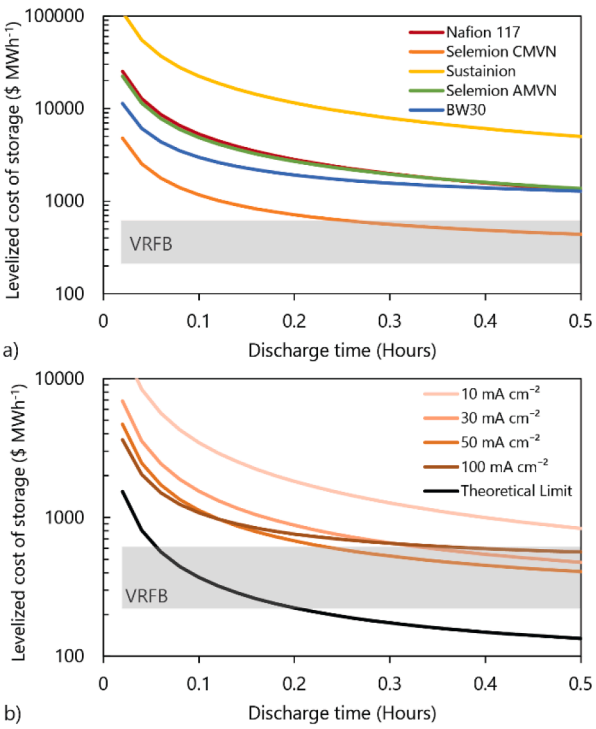

Fig. 7. (a) Levelized cost of storage for short-duration discharge of each membrane studied. Power density used was 30% of peak power density and energy density used was the experimental energy density (Fig. 2a and b). Range of LCOS of vanadium redox flow battery (VRFB) for comparison. (b) Levelized cost of storage for short-duration discharge of Selemion CMVN at different applied current densities using experimental results (Fig. 3a and b) and theoretical limits of peak power density (84 mW cm^{-2}) and energy density (9 Wh L^{-1}).

the lowest cost for long-duration energy scenarios, operation of the Cu_{aq}-TRAB for long durations and a few cycles per year was more expensive ($2560 per MWh) and therefore is not recommended given the current battery setup (Fig. S7). The LCOS of Sustainion was the highest of all membranes studied, despite its high power densities because the membrane cost is by far the most expensive at 10 times the cost of Nafion 117 and 30 times the cost of the Selemion membranes (Table 1). Sustainion is the only membrane tested that is not yet produced commercially; thus, if its production were to be scaled and the cost were reduced, then the membrane would be more cost competitive. Nafion 117, Selemion AMVN, and BW30 showed similar LCOSs for the short discharge times despite Nafion 117 having higher power and energy density because Selemion AMVN and BW30 are inexpensive materials. The convergence in LCOS of these three materials was a result of the degradation rates and cycles efficiency being taken into account in the cost analysis.

The Selemion CMVN was the only membrane to have an LCOS within the range of the vanadium redox flow battery (VRFB) for discharge times longer than 0.25 hours. While VRFBs have much larger power and energy densities than the Cu_{aq}-TRAB using Selemion CMVN, the low material cost of the Cu_{aq}-TRAB components helps drive down the LCOS to similar levels, demonstrating the significant advancement of the Cu_{aq}-TRAB through this work. It has been shown that chloride is a cheaper ligand than bromide [27], but it is unknown how this modification would change battery power and energy, with initial studies indicating poorer performance [26]. However, this highlights how impactful new electrolyte chemistries can be for this space.

Operation of Selemion CMVN at current densities above 30 mA cm^{-2} was found to greatly reduce the LCOS due to the large increases in power density (Fig. 7b). At shorter discharge times, higher applied current reduced costs per MWh due to the higher power output of the battery. As the discharge time grew, the lower applied current densities became less expensive because energy density became more of the total cost for longer discharge times. At the longest discharge time studied (0.50 h), the LCOS at 50 mA cm^{-2} was minimized to $410 per MWh, which was 15% cheaper than operation at 30 mA cm^{-2}. Thereby demonstrating that the optimal operating current density for LCOS was consistent with electrochemical testing where 50 mA cm^{-2} operation had a combination of high power and energy density (Fig. 3b). These results suggest that thinner versions of Nafion such as 115 or 212 could be viable (lower LCOS) despite higher ammonia flux because, to a certain degree, power density increases are more important than energy density decreases.

For the Cu_{aq}-TRAB to be considered cost-effective, longer discharge times and higher current operation is necessary, and at these conditions, the LCOS of the Cu_{aq}-TRAB was found to be near the average of that of a VRFB. A comparison to a VRFB is presented here because the technologies are similar and VRFBs are currently being installed at commercial scale, not because the technologies are competitors in the same market. Naturally, the LCOS when using the current power and energy density limits of the Cu_{aq}-TRAB were much lower than experimental results, with the minimum LCOS being $134 per MWh. Increasing power and energy density to these levels could be achieved through means such as continued reduction of system ohmic losses, increasing operating temperature [24,56], improvement of mass transfer through different cell architectures [32,57] and electrodes [19,58–60], and increased open circuit potential [9].

4. Conclusions

A hydrocarbon cation exchange membrane (Selemion CVMN) was found to be the highest performing membrane tested in the Cu_{aq}-TRAB when considering a combination of lower material cost, electrical resistance, and lower ammonia crossover. Its peak power density was 84 mW cm^{-2}, with an average power density of 26 ± 7 mW cm^{-2} when discharging at 50 mA cm^{-2} to provide 2.9 Wh L^{-1} of energy. Diffusion tests showed that ammonium had the highest flux of all ions measured, even in anion exchange membranes. However, membrane charge was related to the degree to which cations or anions were passed with ammonium flux being an order of magnitude greater than bromide for cation membranes, but only 2-3 times greater for anion membranes. Water uptake showed some relationship to performance for charged membranes, but ionic flux was a better indicator of power density. Correlation of symmetry cell to full cell performance shows that membranes which provide a balance of low resistance and low basic species flux will result in high power and energy density. Economic analysis showed that operation of the Cu_{aq}-TRAB with Selemion CMVN was cost competitive with commercial large scale energy systems, with the levelized cost of storage being as low as $410 per MWh for short-discharge applications.

CRediT authorship contribution statement

Nicholas R. Cross: Methodology, Investigation, Visualization, Validation, Writing – original draft. **Holkan Vazquez-Sanchez:** Methodology, Investigation, Visualization, Validation, Writing – original draft. **Matthew J. Rau:** Conceptualization, Supervision, Methodology, Writing – review & editing. **Serguei N. Lvov:** Methodology, Supervision, Writing – review & editing. **Michael A. Hickner:** Methodology, Writing – review & editing. **Christopher A. Gorski:** Methodology, Writing – review & editing. **Shashank S. Nagaraja:** Methodology, Writing – review & editing. **S. Mani Sarathy:** Methodology, Writing – review & editing. **Bruce E. Logan:** Conceptualization, Methodology, Writing – review & editing. **Derek M. Hall:** Funding acquisition, Supervision, Conceptualization, Methodology, Writing – review & editing.

Declaration of Competing Interest

The authors declare that they have no known competing financial interests or personal relationships that could have appeared to influence the work reported in this paper.

Data availability

Data will be made available on request.

Acknowledgments

This material is based upon work supported by the Department of Energy under Award Number DE-FE0032030. The authors would like to thank Renaldo Springer for his help measuring copper species crossover.

Supplementary materials

Supplementary material associated with this article can be found, in the online version, at doi:10.1016/j.electacta.2023.143090.

References

[1] A. Firth, B. Zhang, A. Yang, Quantification of global waste heat and its environmental effects, Appl. Energy 235 (2019) 1314–1334, https://doi.org/10.1016/j.apenergy.2018.10.102.
[2] D. Brogioli, F.La Mantia, Innovative technologies for energy production from low temperature heat sources: critical literature review and thermodynamic analysis, Energy Environ. Sci. (2021) 1057–1082, https://doi.org/10.1039/d0ee02795b.
[3] D. Brogioli, F.La Mantia, Electrochemical methods for exploiting low-temperature heat sources: challenges in material research, Adv. Energy Mater. 12 (2022), 2103842, https://doi.org/10.1002/aenm.202103842.
[4] D. Huo, H. Tian, G. Shu, W. Wang, Progress and prospects for low-grade heat recovery electrochemical technologies, Sustain. Energy Technol. Assess. 49 (2022), 101802, https://doi.org/10.1016/j.seta.2021.101802.
[5] A. Battistel, P. Peljo, Recent trends in thermoelectrochemical cells and thermally regenerative batteries, Curr. Opin. Electrochem. 30 (2021), 100853, https://doi.org/10.1016/j.coelec.2021.100853.
[6] C. Cheng, Y. Dai, J. Yu, C. Liu, S. Wang, S.P. Feng, M. Ni, Review of liquid-based systems to recover low-grade waste heat for electrical energy generation, Energy Fuels 35 (2021) 161–175, https://doi.org/10.1021/acs.energyfuels.0c03733.
[7] M. Rahimi, A.P. Straub, F. Zhang, X. Zhu, M. Elimelech, C.A. Gorski, B.E. Logan, Emerging electrochemical and membrane-based systems to convert low-grade heat to electricity, Energy Environ. Sci. 11 (2018) 276–285, https://doi.org/10.1039/c7ee03026f.
[8] N.R. Cross, M.J. Rau, S.N. Lvov, C.A. Gorski, B.E. Logan, D.M. Hall, Power and energy capacity tradeoffs in an all-aqueous copper thermally regenerative ammonia battery, J. Power Sources 531 (2022), 231339, https://doi.org/10.1016/j.jpowsour.2022.231339.
[9] M. Rahimi, A. D'Angelo, C.A. Gorski, O. Scialdone, B.E. Logan, Electrical power production from low-grade waste heat using a thermally regenerative ethylenediamine battery, J. Power Sources 351 (2017) 45–50, https://doi.org/10.1016/j.jpowsour.2017.03.074.
[10] P. Peljo, D. Lloyd, N. Doan, M. Majaneva, K. Kontturi, Towards a thermally regenerative all-copper redox flow battery, Phys. Chem. Chem. Phys. 16 (2014) 2831–2835, https://doi.org/10.1039/c3cp54585g.
[11] S. Maye, H.H. Girault, P. Peljo, Thermally regenerative copper nanoslurry flow batteries for heat-to-power conversion with low-grade thermal energy, Energy Environ. Sci. 13 (2020) 2191–2199, https://doi.org/10.1039/d0ee01590c.
[12] B. Kratochvil, K.R. Betty, A secondary battery based on the copper(II)-(I) and (I)-(0) couples in acetonitrile, J. Electrochem. Soc. 121 (1974) 851, https://doi.org/10.1149/1.2401935.
[13] F. Zhang, J. Liu, W. Yang, B.E. Logan, A thermally regenerative ammonia-based battery for efficient harvesting of low-grade thermal energy as electrical power, Energy Environ. Sci. 8 (2015) 343–349, https://doi.org/10.1039/c4ee02824d.
[14] M. Rahimi, T. Kim, C.A. Gorski, B.E. Logan, A thermally regenerative ammonia battery with carbon-silver electrodes for converting low-grade waste heat to electricity, J. Power Sources. 373 (2018) 95–102, https://doi.org/10.1016/j.jpowsour.2017.10.089.
[15] V.M. Palakkal, T. Nguyen, P. Nguyen, M. Chernova, J.E. Rubio, G. Venugopalan, M. Hatzell, X. Zhu, C.G. Arges, High power thermally regenerative ammonia-copper redox flow battery enabled by a zero gap cell design, low-resistant membranes, and electrode coatings, ACS Appl. Energy Mater. 3 (2020) 4787–4798, https://doi.org/10.1021/acsaem.0c00400.
[16] Y. Zhang, Y. Shi, L. Zhang, J. Li, Q. Fu, X. Zhu, Q. Liao, A fluidized-bed reactor for enhanced mass transfer and increased performance in thermally regenerative batteries for low-grade waste heat recovery, J. Power Sources 495 (2021), 229815, https://doi.org/10.1016/j.jpowsour.2021.229815.
[17] N.R. Cross, D.M. Hall, S.N. Lvov, B.E. Logan, M.J. Rau, The impact of fiber arrangement and advective transport in porous electrodes for silver-based thermally regenerated batteries, Electrochim. Acta 388 (2021), 138527, https://doi.org/10.1016/j.electacta.2021.138527.
[18] Y. Shi, L. Zhang, J. Li, Q. Fu, X. Zhu, Q. Liao, Y. Zhang, 3D printed gradient porous composite electrodes improve anodic current distribution and performance in thermally regenerative flow battery for low-grade waste heat recovery, J. Power Sources 473 (2020), 228525, https://doi.org/10.1016/j.jpowsour.2020.228525.
[19] P. Chen, Y. Shi, L. Zhang, J. Li, X. Zhu, Q. Fu, Q. Liao, Performance of a thermally regenerative battery with 3D-printed Cu/C composite electrodes: effect of electrode pore size, Ind. Eng. Chem. Res. 2020 (2020) 21286–21293, https://doi.org/10.1021/acs.iecr.0c03937.
[20] L. Zhang, Y. Li, X. Zhu, J. Li, Q. Fu, Q. Liao, Z. Wei, Copper foam electrodes for increased power generation in thermally regenerative ammonia-based batteries for low-grade waste heat recovery, Ind. Eng. Chem. Res. 58 (2019) 7408–7415, https://doi.org/10.1021/acs.iecr.9b00616.
[21] W. Wang, H. Tian, G. Shu, D. Huo, F. Zhang, X. Zhu, A bimetallic thermally regenerative ammonia-based battery for high power density and efficiently harvesting low-grade thermal energy, J. Mater. Chem. A 7 (2019) 5991–6000, https://doi.org/10.1039/c8ta10257k.
[22] W. Wang, G. Shu, H. Tian, D. Huo, X. Zhu, A bimetallic thermally-regenerative ammonia-based flow battery for low-grade waste heat recovery, J. Power Sources 424 (2019) 184–192, https://doi.org/10.1016/j.jpowsour.2019.03.086.
[23] W. Wang, H. Tian, D. Huo, S. Yang, S. Li, X. Zhu, G. Shu, Modelling of a bimetallic thermally-regenerative ammonia flow battery for conversion efficiency and performance evaluation, J. Power Sources 499 (2021), 229943, https://doi.org/10.1016/j.jpowsour.2021.229943.
[24] W. Wang, D. Huo, H. Tian, X. Zhu, G. Shu, Temperature characteristics of a copper/zinc thermally-regenerative ammonia battery, Electrochim. Acta 357 (2020), 136860, https://doi.org/10.1016/j.electacta.2020.136860.
[25] W. Wang, S. Yang, D. Huo, H. Tian, S. Li, X. Zhu, G. Shu, Understanding the reaction mechanism and self-discharge of a bimetallic thermally-regenerative ammonia battery, Electrochim. Acta 370 (2021), 137724, https://doi.org/10.1016/j.electacta.2021.137724.
[26] R. Springer, N.R. Cross, S.N. Lvov, B.E. Logan, C.A. Gorski, D.M. Hall, An All-Aqueous Thermally Regenerative Ammonia Battery Chemistry Using Cu(I, II) Redox Reactions, J. Electrochem. Soc. 168 (2021), 070523, https://doi.org/10.1149/1945-7111/ac1030.
[27] H. Vazquez-Sanchez, S.N. Shashank, N.R. Cross, D.M. Hall, S.M. Sarathy, A techno-economic analysis of a thermally regenerative ammonia-based battery, Appl. Energy 347 (2023), 121501, https://doi.org/10.1016/j.apenergy.2023.121501.
[28] N.R. Cross, M.J. Rau, S.N. Lvov, C.A. Gorski, B.E. Logan, D.M. Hall, System efficiency and power assessment of the all-aqueous copper thermally regenerative ammonia battery, Appl. Energy 339 (2023), 120959, https://doi.org/10.1016/j.apenergy.2023.120959.
[29] W. Wang, G. Shu, X. Zhu, H. Tian, Decoupled electrolytes towards enhanced energy and high temperature performance of thermally regenerative ammonia batteries, J. Mater. Chem. A 8 (2020) 12351–12360, https://doi.org/10.1039/d0ta03236k.
[30] Z. Lu, Y. Shi, L. Zhang, Y. Li, J. Li, Q. Fu, X. Zhu, Q. Liao, Ammonia crossover in thermally regenerative ammonia-based batteries for low-grade waste heat recovery, J. Power Sources. 548 (2022), 232085, https://doi.org/10.1016/j.jpowsour.2022.232085.
[31] Y. Zhang, Y. Shi, L. Zhang, J. Li, Q. Fu, X. Zhu, Q. Liao, Graphene oxide modified membrane for alleviated ammonia crossover and improved electricity generation in thermally regenerative batteries, Chin. Chem. Lett. 34 (2022), 107704, https://doi.org/10.1016/j.cclet.2022.07.047.
[32] Y. Shi, L. Zhang, Y. Zhang, J. Li, Q. Fu, X. Zhu, Q. Liao, A self-stratified thermally regenerative battery using nanoprism cu covering ni electrodes for low-grade waste heat recovery, J. Phys. Chem. Lett. 14 (2023) 1663–1673, https://doi.org/10.1021/acs.jpclett.2c03687.
[33] Y. Shi, D. Li, Y. An, L. Zhang, J. Li, Q. Fu, X. Zhu, Q. Liao, Power generation enhancement of a membrane-free thermally regenerative battery induced by the density difference of electrolytes, Appl. Energy 344 (2023), 121302, https://doi.org/10.1016/j.apenergy.2023.121302.
[34] Y. Shi, Y. Li, L. Zhang, J. Li, Q. Fu, X. Zhu, Q. Liao, Development of a membrane-less microfluidic thermally regenerative ammonia-based battery towards small-scale low-grade thermal energy recovery, Appl. Energy 326 (2022), 119976, https://doi.org/10.1016/j.apenergy.2022.119976.
[35] F. Vicari, A. Galia, O. Scialdone, Development of a membrane-less microfluidic thermally regenerative ammonia battery, Energy 225 (2021), 120221, https://doi.org/10.1016/j.energy.2021.120221.
[36] M. Rahimi, L. Zhu, K.L. Kowalski, X. Zhu, C.A. Gorski, M.A. Hickner, B.E. Logan, Improved electrical power production of thermally regenerative batteries using a poly(phenylene oxide) based anion exchange membrane, J. Power Sources 342 (2017) 956–963, https://doi.org/10.1016/j.jpowsour.2017.01.003.
[37] T. Okada, Y. Ayato, M. Yuasa, I. Sekine, The effect of impurity cations on the transport characteristics of perfluorosulfonated ionomer membranes, J. Phys. Chem. B 103 (1999) 3315–3322, https://doi.org/10.1021/jp983762d.
[38] R. Halseid, P.J.S. Vie, R. Tunold, Influence of Ammonium on conductivity and water content of nafion 117 membranes, J. Electrochem. Soc. 151 (2004) A381, https://doi.org/10.1149/1.1641035.
[39] K. Hongsirikarn, J.G. Goodwin, S. Greenway, S. Creager, Influence of ammonia on the conductivity of Nafion membranes, J. Power Sources 195 (2010) 30–38, https://doi.org/10.1016/j.jpowsour.2009.07.013.
[40] S.E. Waters, J.R. Thurston, R.W. Armstrong, B.H. Robb, M.P. Marshak, D. Reber, Holistic design principles for flow batteries: cation dependent membrane resistance

and active species solubility, J. Power Sources 520 (2022), 230877, https://doi.org/10.1016/j.jpowsour.2021.230877.
[41] A.Z. Weber, J. Newman, Transport in polymer-electrolyte membranes, J. Electrochem. Soc. 150 (2003) A1008, https://doi.org/10.1149/1.1580822.
[42] A. Daniilidis, D.A. Vermaas, R. Herber, K. Nijmeijer, Experimentally obtainable energy from mixing river water, seawater or brines with reverse electrodialysis, Renew. Energy 64 (2014) 123–131, https://doi.org/10.1016/j.renene.2013.11.001.
[43] A.M. Pezeshki, Z.J. Tang, C. Fujimoto, C.-N. Sun, M.M. Mench, T.A. Zawodzinski, Full cell study of diels alder poly(phenylene) anion and cation exchange membranes in vanadium redox flow batteries, J. Electrochem. Soc. 163 (2016) A5154–A5162, https://doi.org/10.1149/2.0201601jes.
[44] J. Sun, X. Li, X. Xi, Q. Lai, T. Liu, H. Zhang, The transfer behavior of different ions across anion and cation exchange membranes under vanadium flow battery medium, J. Power Sources 271 (2014) 1–7, https://doi.org/10.1016/j.jpowsour.2014.07.111.
[45] X. Teng, Y. Guo, D. Liu, G. Li, C. Yu, J. Dai, A polydopamine-coated polyamide thin film composite membrane with enhanced selectivity and stability for vanadium redox flow battery, J. Memb. Sci. 601 (2020), 117906, https://doi.org/10.1016/j.memsci.2020.117906.
[46] Q. Dai, Z. Liu, L. Huang, C. Wang, Y. Zhao, Q. Fu, A. Zheng, H. Zhang, X. Li, Thin-film composite membrane breaking the trade-off between conductivity and selectivity for a flow battery, Nat. Commun. 11 (2020) 1–9, https://doi.org/10.1038/s41467-019-13704-2.
[47] X. Zhu, M. Rahimi, C.A. Gorski, B. Logan, A thermally-regenerative ammonia-based flow battery for electrical energy recovery from waste heat, ChemSusChem 9 (2016) 873–879, https://doi.org/10.1002/cssc.201501513.
[48] M. Engelpracht, M. Kohrn, D. Tillmanns, J. Seiler, A. Bardow, Waste heat to power: full-cycle analysis of a thermally regenerative flow battery, Energy Technol. 2200152 (2022), 2200152, https://doi.org/10.1002/ente.202200152.
[49] F. Vicari, A. D'Angelo, Y. Kouko, A. Loffredi, A. Galia, O. Scialdone, On the regeneration of thermally regenerative ammonia batteries, J. Appl. Electrochem. 48 (2018) 1381–1388, https://doi.org/10.1007/s10800-018-1240-0.
[50] J. Luo, Z. Wang, H. Wu, S. Zhang, Vapor pressure measurement of electrolyte solution and its impact on regeneration process in TRAB, Case Stud. Therm. Eng. 36 (2022), 102201, https://doi.org/10.1016/j.csite.2022.102201.
[51] B. Jiang, L. Wu, L. Yu, X. Qiu, J. Xi, A comparative study of nafion series membranes for vanadium redox flow batteries, J. Memb. Sci. 510 (2016) 18–26, https://doi.org/10.1016/j.memsci.2016.03.007.
[52] E.R. Nightingale, Phenomenological theory of ion solvation. Effective radii of hydrated ions, J. Phys. Chem. 63 (1959) 1381–1387, https://doi.org/10.1021/j150579a011.
[53] J. Xi, B. Jiang, L. Yu, L. Liu, Membrane evaluation for vanadium flow batteries in a temperature range of −20–50°C, J. Memb. Sci. 522 (2017) 45–55, https://doi.org/10.1016/j.memsci.2016.09.012.
[54] J.H. Choi, S.H. Kim, S.H. Moon, Heterogeneity of ion-exchange membranes: the effects of membrane heterogeneity on transport properties, J. Colloid Interface Sci. 241 (2001) 120–126, https://doi.org/10.1006/jcis.2001.7710.
[55] R. Yadav, P.S. Fedkiw, Analysis of EIS technique and nafion 117 conductivity as a function of temperature and relative humidity, J. Electrochem. Soc. 159 (2012) B340–B346, https://doi.org/10.1149/2.104203jes.
[56] F. Zhang, N. LaBarge, W. Yang, J. Liu, B.E. Logan, Enhancing low-grade thermal energy recovery in a thermally regenerative ammonia battery using elevated temperatures, ChemSusChem 8 (2015) 1043–1048, https://doi.org/10.1002/cssc.201403290.
[57] H. Tian, W. Jiang, G. Shu, W. Wang, D. Huo, M.Z. Shakir, Analysis and optimization of thermally-regenerative ammonia-based flow battery based on a 3D model, J. Electrochem. Soc. 166 (2019) A2814–A2825, https://doi.org/10.1149/2.0711912jes.
[58] Y. Shi, L. Zhang, Y. Zhang, J. Li, Q. Fu, X. Zhu, Construction of a hierarchical porous surface composite electrode by dynamic hydrogen bubble template electrodeposition for ultrahigh-performance thermally regenerative ammonia-based batteries, Chem. Eng. J. 423 (2021), 130339, https://doi.org/10.1016/j.cej.2021.130339.
[59] P. Chen, L. Zhang, Y. Shi, J. Li, Q. Fu, X. Zhu, Z. Lu, Q. Liao, Biomass waste-derived hierarchical porous composite electrodes for high-performance thermally regenerative ammonia-based batteries, J. Power Sources 517 (2022), 230719, https://doi.org/10.1016/j.jpowsour.2021.230719.
[60] Y. Shi, Y. An, Z. Tang, L. Zhang, J. Li, Q. Fu, X. Zhu, Q. Liao, Electrical power production of thermally regenerative ammonia-based batteries using reduced graphene oxide modified Ni foam composite electrodes, Appl. Energy 326 (2022), 119966, https://doi.org/10.1016/j.apenergy.2022.119966.